Supplementary Information

Deficient neuron-microglia signaling results in impaired functional brain connectivity and social behavior

Yang Zhan[1]*, Rosa C. Paolicelli[1]*, Francesco Sforazzini[2,3], Laetitia Weinhard[1], Giulia Bolasco[1], Francesca Pagani[4], Alexei L. Vyssotski[5], Angelo Bifone[2], Alessandro Gozzi[2], Davide Ragozzino[6,7], and Cornelius T. Gross[1]†

[1] Mouse Biology Unit, European Molecular Biology Laboratory (EMBL), Via Ramarini 32, 00015 Monterotondo, Italy

[2] Center for Neuroscience and Cognitive Systems @UniTn, Istituto Italiano di Tecnologia, (IIT), Rovereto, Italy

[3]IMT - Institute for Advanced Studies Lucca, Italy

[4] Center for Life Nano Science, IIT, La Sapienza University, Rome, Italy

[5] Institute of Neuroinformatics, University of Zürich and Swiss Federal Institute of Technology (ETH), Winterthurerstr. 190, 8057 Zurich, Switzerland

[6] Department of Physiology and Pharmacology, La Sapienza University, Rome, Italy

[7] IRCCS Neuromed, Pozzilli, Italy

* Equal contribution

† To whom correspondence should be addressed: gross@embl.it

Nature Neuroscience: doi:10.1038/nn.3641

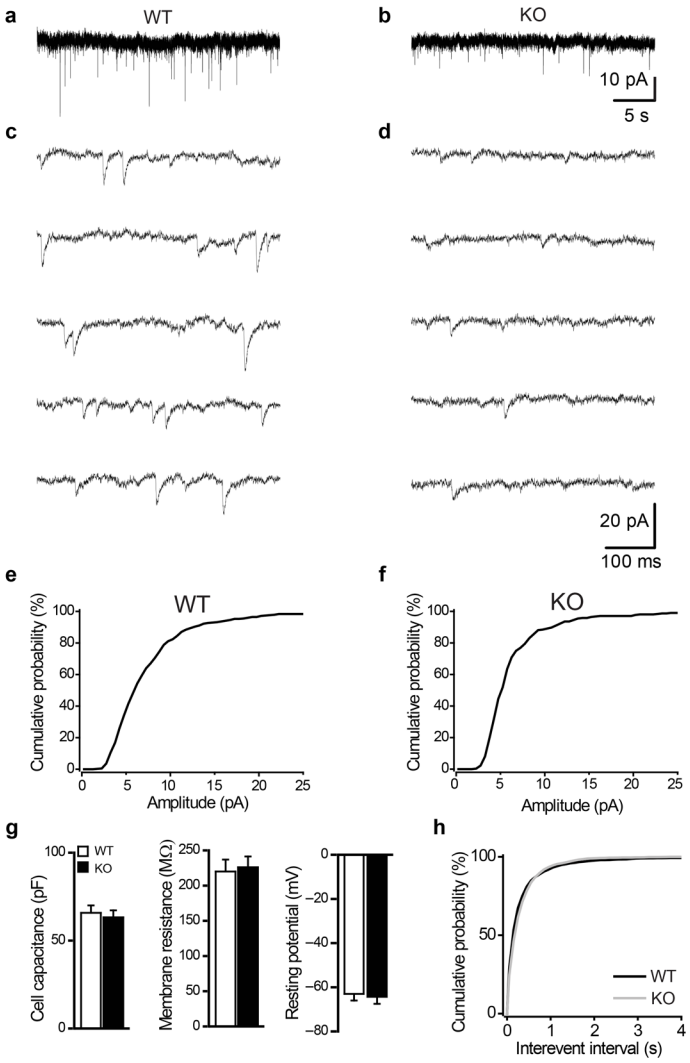

Supplementary Figure 1. In vitro **electrophysiology.** (**a**,**b**) Representative traces of patch clamp electrophysiological recordings from CA1 hippocampal neurons from wild-type and *Cx3cr1*^{KO} mice. (**c,d**) Sample synaptic events recorded from neurons in wild-type and *Cx3cr1*^{KO} mice. Noise amplitude, estimated as peak-to-peak amplitude in 5 ms segments of 1kHz filtered traces by Clampfit 10 software, was not statistically different in wild-type and *Cx3cr1*^{KO} mice (*t* test; WT, 3.7 ± 0.3 pA, *n* = 14/14/5 cells/slices/mice; KO, 4.0 ± 0.3 pA, *n* = 14/12/5; *P* = 0.44). (**e**,**f**) Cumulative distributions of sEPSC from the same cells in (**a**,**b**). Wild-type mice displayed frequent large events whereas *Cx3cr1*^{KO} mice showed few. (**g**) Passive properties of neurons in wild-type and *Cx3cr1*^{KO} mice. Cell capacitance and resistance values were provided by Clampex 10 acquisition software. Resting potential was estimated from zero current potential -the potential imposed to the cell to zero the pipette offset after the membrane rupture. The mean values reported for all passive properties are not statistically different (*t* test; cell capacitance: WT, *n* = 18/16/4; KO, *n* = 17/14/5, *P* = 0.65; cell resistance: WT, *n* = 20/18/5; KO, *n* = 17/14/5, *P* = 0.79; resting potential: WT, *n* = 17/15/5; KO, *n* = 9/8/5, *P* = 0.79). (**h**) Inter-event distributions of mIPSCs in wild-type (black line) and *Cx3cr1*^{KO} (gray line) littermate mice at PND15 (WT, *n* = 22/17/4; KO, *n* = 23/16/5; *D* = 0.07, *P* < 0.00001). The frequency of mIPSCs was slightly higher in wild-type compared to *Cx3cr1*^{KO} neurons (*t* test;WT, 4.2 ± 0.5 Hz; KO, 3.3 ± 0.2 Hz; *P* = 0.045).

Nature Neuroscience: doi:10.1038/nn.3641

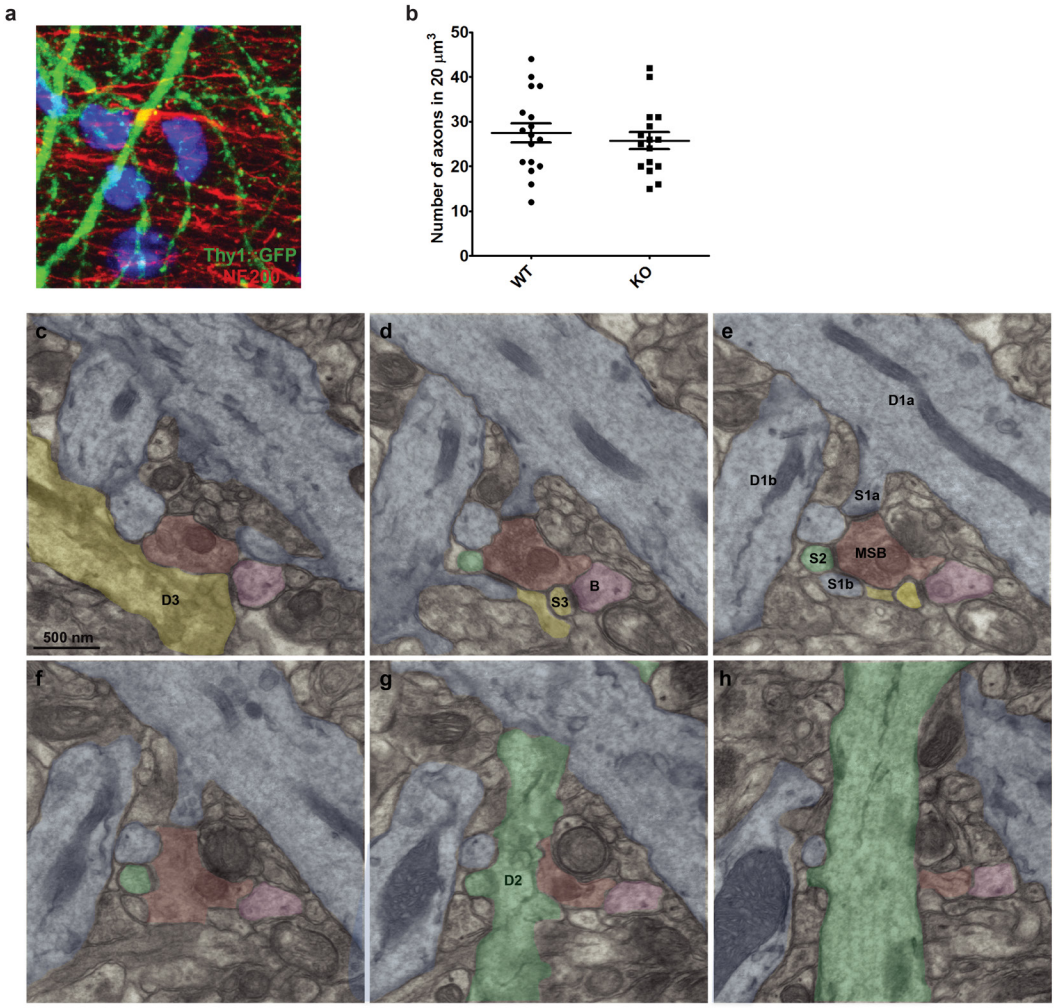

Supplementary Figure 2. **Light and electron microscopy.** (**a**) Representative image of NF-200-positive axons in CA1 *stratum radiatum.* The *Thy1*::GFP transgene labels sparse neuronal dendrites. Blue indicates DAPI nuclear staining. (**b**) Quantification of the number of NF-200-positive processes did not reveal any significant difference in axonal density between wild-type and *Cx3cr1*^{KO} littermates (*t* test; WT: $n = 17$ sections from 3 animals, KO: $n = 16$ sections from 3 animals, $P = 0.56$). (**c–h**). Serial electron microscope sections showing an example of a multi-synapse bouton (MSB) making excitatory synapses with three neighboring dendritic spines (S1a, S1b, S2) emanating from three distinct dendritic shafts (D1a, D1b, and D2), two of which derive from the same target neuron (D1a, D1b). In addition, a single-synapse bouton (B) is seen making an excitatory synapse with a single dendritic spine (S3) protruding from a fourth dendrite (D3).

Nature Neuroscience: doi:10.1038/nn.3641

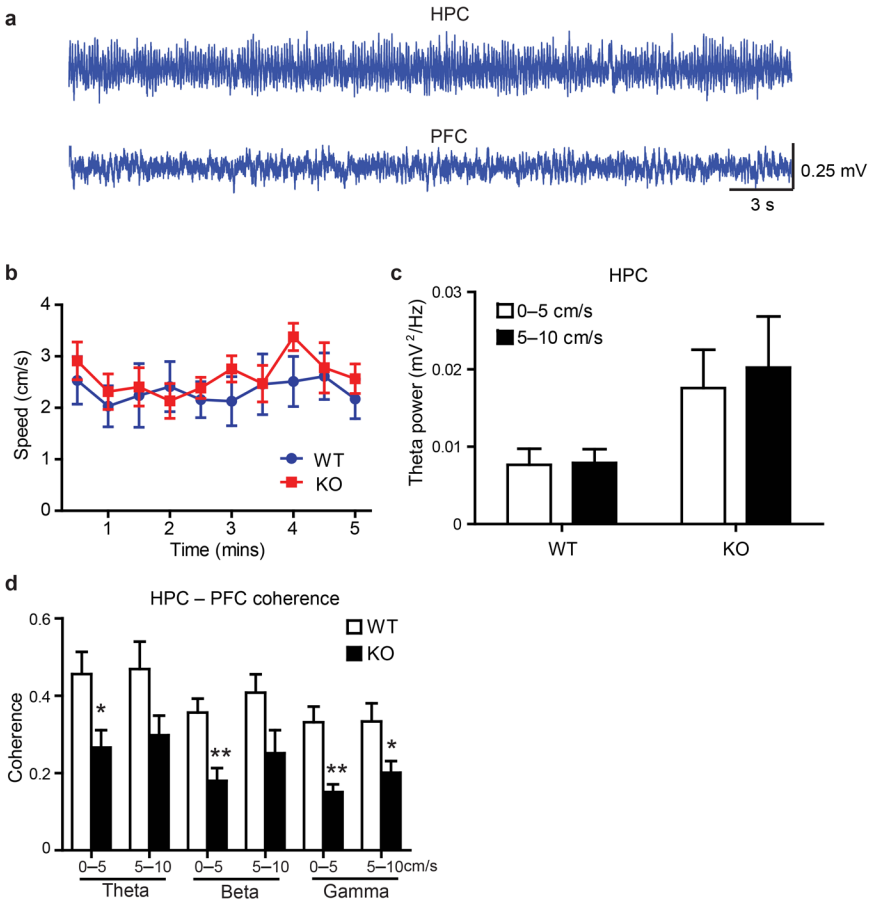

***Supplementary Figure 3. In vivo* electrophysiology.** (**a**) Representative LFP recordings from right hippocampus (top, HPC) and prelimbic cortex (bottom, PFC). Thirty seconds of continuous recording are shown. (**b**) Speed of wild-type and *Cx3cr1*^{KO} littermate mice during 5 minutes habituation to the three-chambered social interaction apparatus. No significant genotype effect on speed was observed. (**c**) Partition of dorsal hippocampal LFP theta power into epochs of low (0–5 cm/s) and high (5–10 cm/s) speed did not reveal a genotype effect on theta power in either speed range. (**d**) The genotype effect on PFC−HPC LFP coherence was maintained following partitioning of the data into low (0–5 cm/s) and high (5–10 cm/s) speed ranges. For panels (**b–d**), WT: $n = 7$; KO: $n = 10$. *$P < 0.05$, **$P < 0.01$.

Nature Neuroscience: doi:10.1038/nn.3641

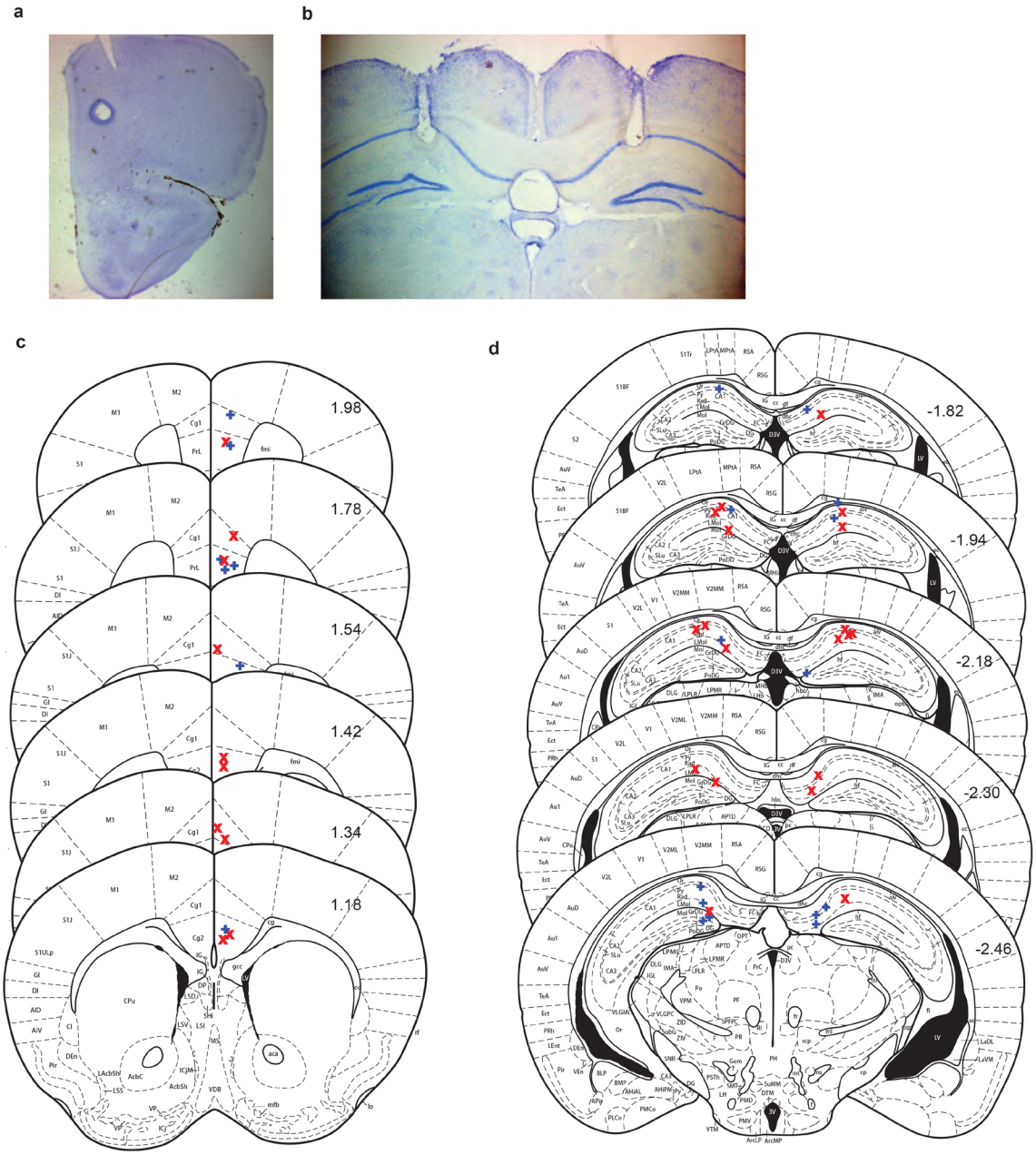

Supplementary Figure 4. **Location of *in vivo* recording electrodes.** Representative Nissl-stained brain sections showing electrolytic lesions produced by LFP electrodes placed in (**a**) dorsal hippocampus (HPC) and (**b**) pre-limbic cortex (PFC). Summary of lesion sites of animals included in the LFP coherence experiments superimposed on coronal brain atlas sections indicates electrode localization to (**c**) dorsal hippocampus and (**d**) pre-limbic/cingulate cortex (+ wild-type, x knockout).

Nature Neuroscience: doi:10.1038/nn.3641

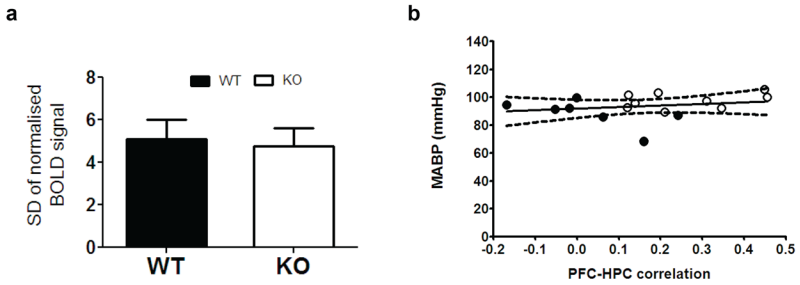

Supplementary Figure 5. **Comparable BOLD signal fluctuation and arterial blood pressure in wild-type and *Cx3cr1*^{KO} mice during rs-fMRI.** (**a**) Analysis of the standard deviation (SD) of normalized rs-fMRI BOLD time series data in somatosensory regions, a parameter inversely correlated with anesthesia depth in rodents, produced comparable inter-strain values (*t* test; WT: $n = 9$; KO: $n = 7$; $P = 0.47$), thus arguing against a differential sensitivity to anesthesia of the two genotypes. (**b**) This was confirmed by a lack of correlation (Pearson correlation; $r^2 = 0.05$, $P = 0.41$) between mean arterial blood pressure (MABP), an additional sensitive indicator of anesthesia depth, and PFC–HPC connectivity. MABP values for the wild-type and *Cx3cr1*^{KO} mice were not different (*t* test; $P = 0.16$. WT: $n = 9$, open circles; KO: $n = 7$, filled circles).

Nature Neuroscience: doi:10.1038/nn.3641

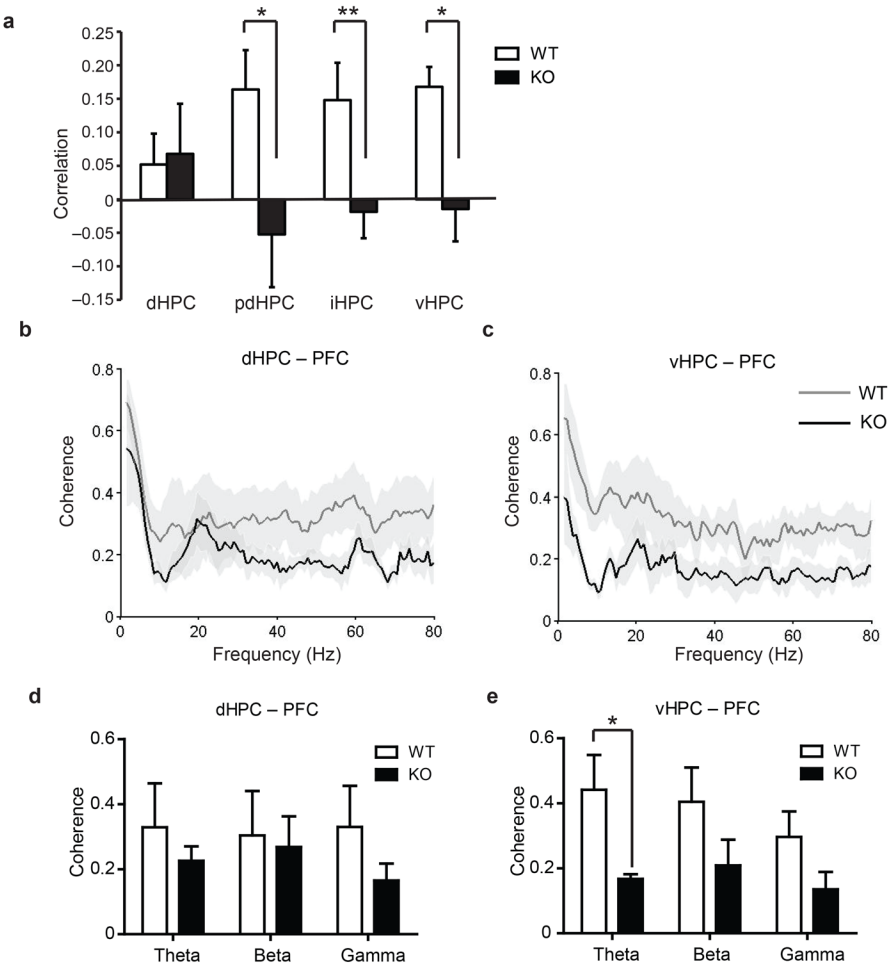

Supplementary Figure 6. **Dorsal-ventral gradient of functional connectivity deficits in *Cx3cr1*^{KO} mice.** (**a**) Correlation of PFC–HPC fMRI BOLD signal in *Cx3cr1*^{KO} mice compared to wild-type littermates showed a gradient from dorsal to ventral hippocampus with greater differences seen in ventral compared to dorsal hippocampal regions (WT: $n = 9$; KO: $n = 7$). PFC–HPC Functional connectivity as assessed by LFP coherence was decreased to a lesser extent in (**b**,**d**) dorsal hippocampus (dHPC) than in (**c**,**e**) ventral hippocampus (WT: $n = 4$; KO: $n = 4$). *$P < 0.05$, ** $P < 0.01$.

Nature Neuroscience: doi:10.1038/nn.3641

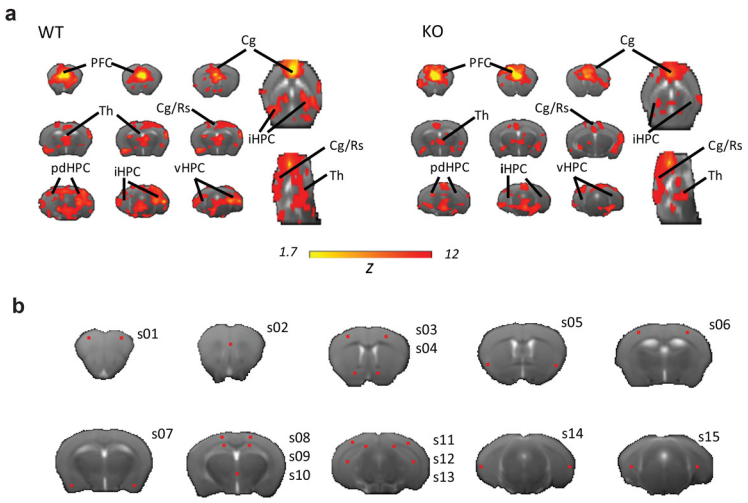

Supplementary Figure 7. **Resting-state fMRI functional connectivity analysis.** (**a**) Heat maps showing correlation (*z*-score) of resting-state fMRI BOLD signal across brain regions viewed in coronal, transverse, and sagittal sections with a seed in pre-limbic cortex (PFC). Note that overall higher correlations are seen in (left) wild-type compared to (right) *Cx3cr1*^{KO} littermates. (**b**) Anatomical location of seed regions (s01–s15) used to construct correlation matrices (s01: Fra – Frontal Association Area, s02: PrL –Pre-limbic Cortex, s03: M1 – Primary Motor Cortex, s04: Acb – Nucleus Accumbens, s05: Ins – Agranular Insular Cortex, s06: SS – Somatosensory Cortex, s07: Amy –Amygdala, s08: PtA – Parietal Association Cortex; s09: dHPC – Dorsal Hippocampus, s10: Re – Nucleus Reuniens, s11: Vis – Visual Cortex, s12: pdHPC – Postero-Dorsal Hippocampus, s13: iHPC – Ventral Hippocampus, s14: TeA – Temporal Association Cortex, s15: vHPC – Postero-Ventral Hippocampus).

Nature Neuroscience: doi:10.1038/nn.3641

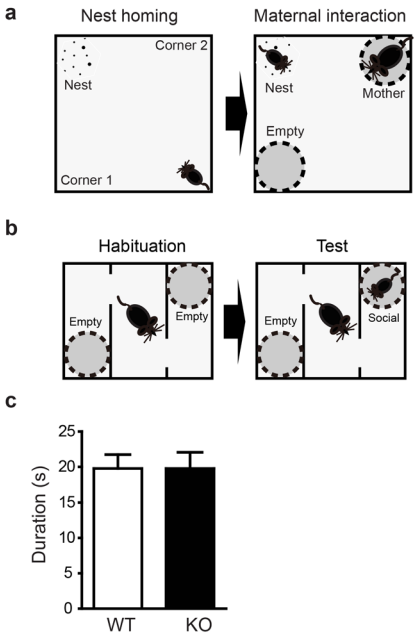

Supplementary Figure 8. **Social interaction tests and grooming behavior.** (**a**, nest homing) Juvenile mice were placed into one corner (start) of a novel open arena filled with fresh bedding and with familiar bedding strewn into the opposite corner (nest) and time spent in each corner (corner 1, corner 2) was recorded during three minutes. Subsequently, the mice were briefly removed while wire mesh tubes were placed into two corners as indicated and the mother was placed into one of the tubes. (**a**, maternal interaction) Time spent sniffing the tubes (empty, mother) was recorded during five minutes. (**b**) Adult mice were placed into a three-chambered apparatus with wire mesh tubes in the outer compartments for 5 minutes (Habituation). Subsequently, the mice were briefly removed while a juvenile mouse was placed into one of the tubes. Time spent in the chamber (empty, social) was recorded during ten minutes (Test). (**c**) Duration of self-grooming during 1 minute following a spray of water to the face was similar in wild-type mice and *Cx3cr1*^{KO} littermates (*t* test; WT: $n = 23$; KO: $n = 14$; $P = 0.99$).

Nature Neuroscience: doi:10.1038/nn.3641

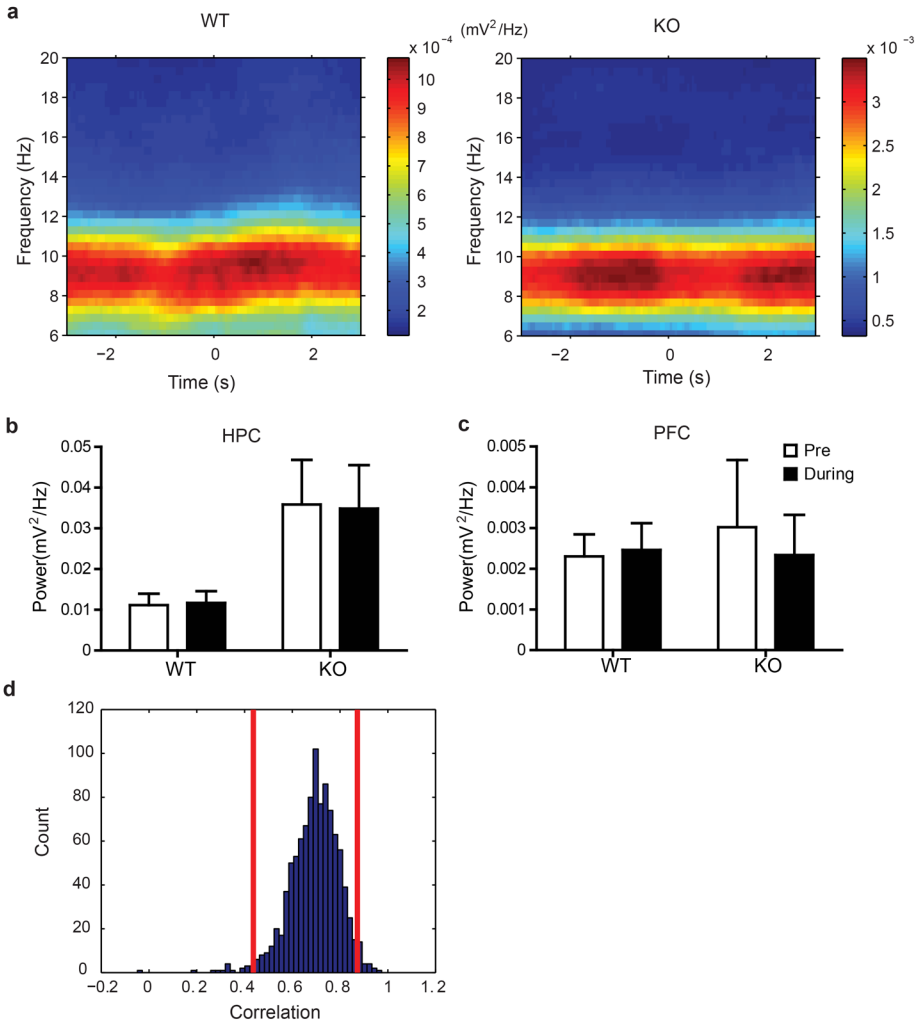

Supplementary Figure 9. **Correlation between LFP coherence and social behavior.** (**a**) Averaged time-dependent HPC power spectra in (left) wild-type and (right) knockout mice during the three seconds preceding and following exploratory contact with the tube containing a juvenile mouse in the social preference test. Neither genotype demonstrated a significant change in theta power in either (**b**) HPC or (**c**) PFC when comparing the pre-stimulus (Pre) and post-stimulus (During) period (paired *t* test; HPC, WT: $n = 7$, $t_6 = 1.1$, $P = 0.3$; KO: $n = 10$, $t_9 = 0.52$, $P = 0.61$. PFC, WT: $n = 7$, $t_6 = 1.04$, $P = 0.34$; KO: $n = 10$, $t_9 = 1.01$, $P = 0.34$). (**d**) Distribution of the correlation between PFC−HPC coherence in the theta band and social interaction time estimated using bootstrap (1000 resamples) method. The 95% confidence interval was [0.43, 0.87].

Nature Neuroscience: doi:10.1038/nn.3641

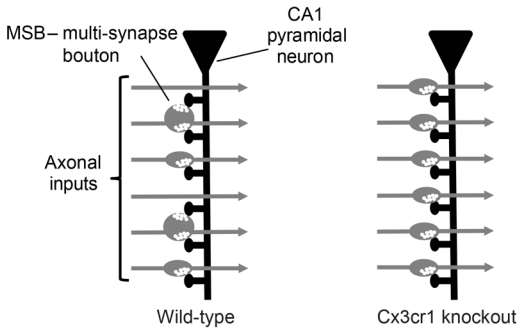

Supplementary Figure 10. **Model for immature synaptic multiplicity in *Cx3cr1*^{KO} mice**. During the first phase of synaptogenesis, each afferent excitatory input makes a single synaptic contact with its target. Action potentials passing down an axon lead to neurotransmitter release at a single synapse. Under these conditions, the amplitude of action potential-dependent synaptic responses (sEPSC) is equivalent to non-action potential-dependent synaptic responses (mEPSC) and synaptic inputs have a unitary multiplicity. Upon completion of synaptogenesis, however, a significant fraction of excitatory inputs makes multiple synaptic contacts with its target via multi-synapse boutons (MSBs, wild-type, left). Action potentials passing down an axon induce simultaneous release at multiple synapses leading to a larger sEPSC, while mEPSC amplitudes remain unaltered. In *Cx3cr1*^{KO} mice microglia are transiently decreased during development and synaptic pruning is impaired. Because synapse elimination is linked to the formation of MSBs, knockout mice form fewer MSBs (right) resulting in immature synaptic multiplicity and weak functional connectivity. Note that, despite divergent multiplicity, the number of axons and spines in the mature circuits of wild-type and *Cx3cr1*^{KO} mice are similar.

Nature Neuroscience: doi:10.1038/nn.3641